Molecular Therapy
Nucleic Acids
Original Article

Deletion of miR-126a Promotes Hepatic Aging and Inflammation in a Mouse Model of Cholestasis

Yi Yan,[1,6] Dan Qin,[1,6] Bian Hu,[2,6] Chunjing Zhang,[1] Shenghui Liu,[1] Dongde Wu,[3] Wendong Huang,[4] Xingxu Huang,[2] Liqiang Wang,[5] Xiangmei Chen,[5] and Lisheng Zhang[1]

[1]College of Veterinary Medicine, Bio-medical Center, Huazhong Agricultural University, Wuhan, Hu Bei 430070, China; [2]School of Life Science and Technology, Shanghai Tech University, 100 Haike Road, Pudong New Area, Shanghai 201210, China; [3]Department of Hepatobiliary and Pancreatic Surgery, Cancer Hospital of Wuhan University (Hubei Cancer Hospital), Wuhan, Hubei 430079, China; [4]Department of Diabetes Complications and Metabolism, Diabetes and Metabolism Research Institute, Beckman Research Institute, City of Hope National Medical Center, Duarte, CA 91010, USA; [5]Department of Nephrology, Chinese PLA General Hospital, Chinese PLA Institute of Nephrology, State Key Laboratory of Kidney Diseases, National Clinical Research Center for Kidney Diseases, 28th Fuxing Road, Beijing 100853, China

MicroRNAs (miRNAs) act as regulators of aging at the tissue or organism level or as regulators of cellular senescence. Targeted deletion of miR-126 in mice causes partial embryonic lethality, but its biological function in the liver is still largely unknown. Here, we deleted miR-126a, using the CRISPR/Cas9 system *in vitro* and *in vivo*. miR-126a was reduced in the aging livers, and disruption of miR-126a in bone mesenchymal stem cells (BMSCs) induced age-associated telomere shortening, DNA damage responses, and proinflammatory cytokines. Moreover, disruption of miR-126a in mice caused hepatocyte senescence, inflammation, and metabolism deficiency. In addition, disruption of miR-126a via BMSC transplantation aggravated the severity of liver defects induced by cholestasis compared with that in the functional miR-126a BMSC group. Mechanistically, we identified versican (VCAN) as a novel direct miR-126a-5p target that induces telomere shortening, BMSC senescence, and nuclear factor κB (NF-κB) pathway activation. This study identified aging-related reduced expression of miR-126a and promotion of its target VCAN as a key mechanism in the regulation of hepatic metabolic function during aging and hepatic damage by inducing NF-κB pathway activation, DNA repair function disorder, and telomere attrition. The findings indicate that miR-126a may be a drug target for the treatment of hepatic failure.

INTRODUCTION

MicroRNAs (miRNAs) are short, non-coding RNA molecules that consist of approximately 22 nt. They play a vital role in regulatory mechanisms of complex physiological and pathological processes, such as proliferation, differentiation, plasticity, senescence, apoptosis, and carcinogenesis.[1–3] Through interactions with 3′ UTRs, miRNAs can modulate the expression of many genes simultaneously, often regulating individual signaling pathways at multiple levels.[4–6]

The role of miRNAs in regulating aging processes has been established, beginning with the report that the founding miRNA, lin-4, regulates lifespan in *C. elegans*.[7] Currently, numerous miRNAs have been identified as regulators of aging at different tissues.[8–10] Moreover, many age-related diseases and aging itself are closely associated with low-level chronic inflammation.[11,12] miRNA has been shown to either promote or delay cellular senescence through regulating the aging-related signaling proteins.[13] Senescence can be triggered by many different mechanisms, including DNA damage, expression of oncogenes, oxidative stress, and telomere shortening.[14,15]

miR-126 is an endothelial-cell-specific miRNA that is encoded in the intron of epidermal-growth-factor-like domain 7. It gives rise to two mature miRNAs, miR-126a-3p and miR-126a-5p,[16] which are a miRNA pair derived from a single precursor. Previous research has shown that targeted deletion of miR-126 in mice causes partial embryonic lethality that is related to a loss of vascular integrity and defects in endothelial cell proliferation, migration, and angiogenesis.[17] However, most of the miRNA-knockout mice have not been shown to be a lethal phenotype, such as miR-34a[10] and miR-122[18] knockout mice. This suggested that miR-126a is critical for the development and growth of organisms.

miR-126 may be transactivated by the ligand-activated transcription factor farnesoid X receptor (FXR).[19] Previous research has shown that FXR is involved in liver regeneration and repair and that activation of FXR largely alleviates age-related liver regeneration defects.[20] This suggests that miR-126 may play roles in the liver aging process.

In this study, we showed that VCAN regulated by miR-126 plays an important role in the aging process. VCAN belongs to the family of large, aggregating chondroitin sulfate proteoglycans located primarily within the extracellular matrix.[21] It is known to be involved in inflammation and prevents T cell binding to soluble hyaluronan, as well as the amoeboid shape change on hyaluronan-coated dishes and T cell penetration of collagen gels.[22] VCAN has also been shown to be

Received 14 June 2018; accepted 4 April 2019;
https://doi.org/10.1016/j.omtn.2019.04.002.

[6]These authors contributed equally to this work.

Correspondence: Lisheng Zhang, College of Veterinary Medicine, Bio-medical Center, Huazhong Agricultural University, Wuhan, Hu Bei 430070, China.
E-mail: lishengzhang@mail.hzau.edu.cn

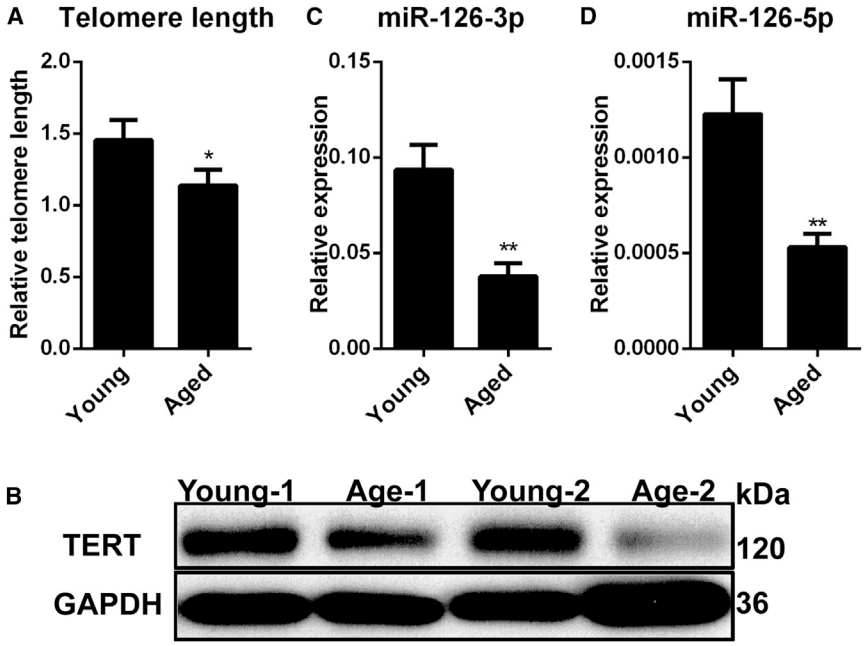

Figure 1. miR-126a Expression Is Low in Aged Livers

(A) Real-time PCR-based telomere length measurement of young and aged livers. Bars represent normalized mean values ± SD. *p < 0.05 by two-tailed Student's t-test. (B) Western blot for TERT protein in aged and young mouse livers; GAPDH was used as a control for the examination of TERT. (C and D) Real-time PCR expression analysis of miR-126a-3p (C) and miR-126a-5p (D) in aged and young mouse livers. U6 small nuclear RNA (snRNA) was used as a control for the detection of mature miR-126a-3p and miR-126a-5p. Bars represent normalized mean values ± SD. **p < 0.01 by two-tailed Student's t-test.

involved in diverse cell functions, such as adhesion, migration, proliferation, and apoptosis.[23]

In this study, disruption of miR-126a by CRISPR/Cas9-mediated genome-editing technology at the DNA level *in vitro* and *in vivo* promoted bone mesenchymal stem cell (BMSC) senescence and hepatic aging and affected the rescuing effect of BMSC transplantation and mouse hepatic function through targeting VCAN, thus activating the NF-κB pathway, which contributes to senescence-associated inflammation and hepatic metabolism.

RESULTS

Downregulation of miR-126a in Aged Mouse Liver

Previous studies reported that miRNA has an important role in aging, and targeted deletion of miR-126a in mice causes partial embryonic lethality, which indicates the importance of miR-126a in growth and development. Additional, activation of FXR largely alleviates age-related liver regeneration defects,[20] and FXR may promote the transcription of miR-126a.[19] Therefore, we focused on the involvement of this miRNA family in the aging process in the liver. As expected, livers of aged mice (13–16 months) showed shorter telomeres (Figure 1A) and decreased telomerase reverse transcriptase (TERT) expression (Figure 1B) than that of the young mice (8 weeks old). Interestingly, the entire miR-126a family (comprising miR-126a-3p and -5p) was significantly downregulated in aged livers (Figures 1C and 1D). Taken together, these results indicate that miR-126a may play a role in the telomere attrition associated with aging.

Disruption of miR-126a Using the CRISPR/Cas9 System *In Vitro* and *In Vivo*

To study the role of miR-126a in aging cells, the miR-126a gene was disrupted, using the CRISPR/Cas9 lentivirus system *in vitro*, and two pairs of guide RNAs (gRNAs) were designed to delete miR-126a. The double gRNAs were expressed in one lentiviral plasmid constructed under two independent U6 promoters (Figure 2A). We initially screened candidate CRISPR gRNAs targeting sequences in sgRNA1 and -3 in mice upstream of the pre-miR-126a gene in NIH 3T3 cells. One of them formed a pair of sgRNAs with sgRNA2. The guide RNA targeting sgRNA3 displayed ~50% mutagenesis at the on-target site in pre-miR-126a, as determined by PCR and a T7 endonuclease 1 (T7EN1) cleavage assay (Figure S1A). Next, we packaged the pre-miR-126a disruption lentiviral vector to co-express Cas9, GFP, and two sgRNAs targeting the mouse pre-miR-126a gene (Figure 2A).

To test this lentivirus expression system, the resulting lentivirus vector was packaged and transduced into HEK293T cells. Then, we transduced lentivirus-control (Lenti.ctrl) and lentivirus-sg126 (Lenti.sg126) into 3T3-L1 cells. PCRs with specific primers confirmed that the expected deletions were obtained with a pair of sgRNA combinations (Figure 2B). The above PCR products were digested by the T7EN1 enzyme after denaturation and annealing. A T7EN1 cleavage assay showed that samples displayed cleavage bands (Figure 2C), and sequencing of PCR products showed that miR-126a was deleted (Figure 2D).

To further establish the role of miR-126a in hepatic aging, we packaged the pre-miR-126a-disrupted adenovirus vector to co-express Cas9, GFP, and two sgRNAs targeting the mouse pre-miR-126a gene (Figure S1B). 3T3-L1 genomic DNA was isolated after adenovirus infection, and the region around the target site was amplified by PCR. PCR and T7EN1 cleavage assays showed that samples displayed cleavage bands (Figure S1C), and sequencing of PCR products showed deletion of pre-miR-126a (Figure S1D). These results validated the miR-126a gene-editing function of adenovirus-sg126. (Ad.sg126).

To examine the gene-editing efficiency *in vivo*, Ad.sg126 was reconstituted in 100 μL injected intravenously through tail vein injection. Liver tissues were harvested after 3 days, and Ad.sg126 mice displayed suitable levels of mutagenesis, as determined by T7EN1 cleavage assay

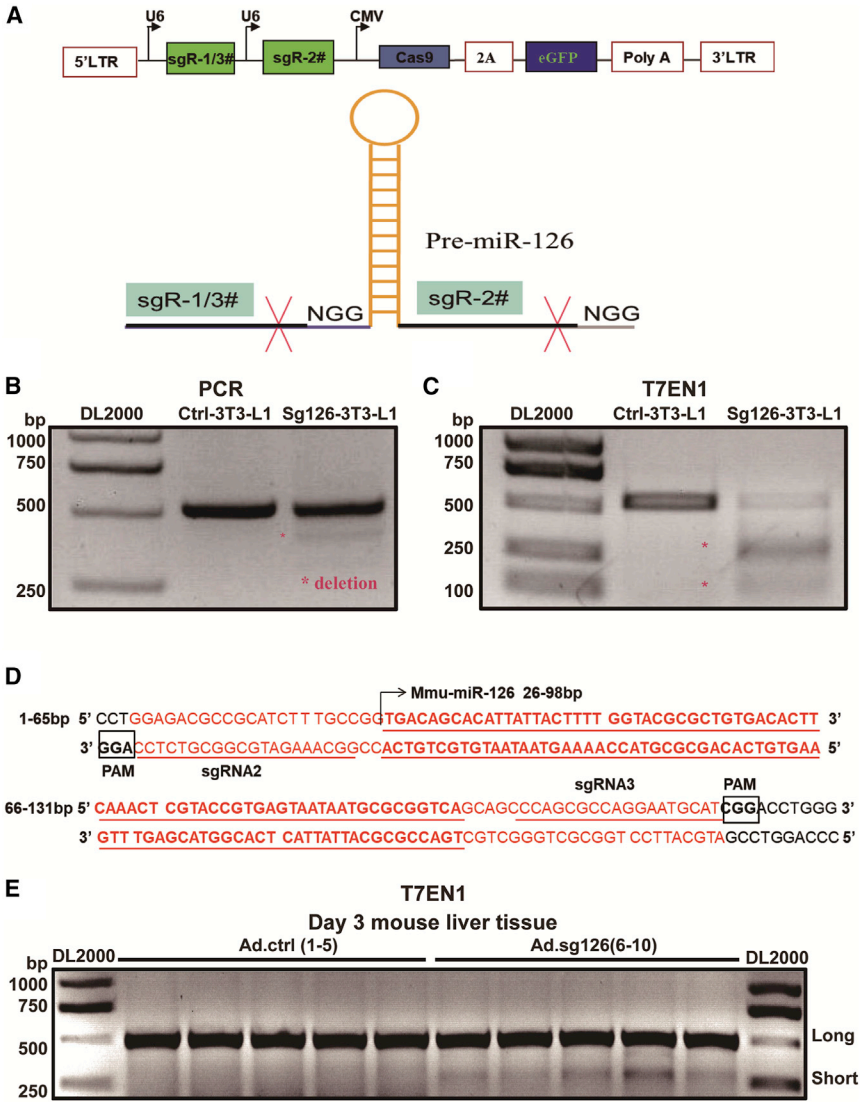

Figure 2. Disruption of miR-126a Using the CRISPR/Cas9 System *In Vitro* and *In Vivo*

(A) Schematic illustration of gRNA expression from the lentiviral vector and the target sites in the genome. The positions of the Sg-126 binding site and protospacer adjacent motif (PAM) are labeled. (B) Detection of miR-126a-deleted genomic sequences in Ctrl-3T3-L1 and Sg126-3T3-L1 by PCR. (C) Detection of sgRNA: Cas9-mediated on-target cleavage of miR-126a confirmed by a T7EN1 cleavage assay in Ctrl-3T3-L1 and Sg126-3T3-L1 cells. (D) Detection of the miR-126a-deleted genomic sequence in Sg126-3T3-L1 cells by sequencing. The sequence of mmu-miR-126a and the positions of sg-126 and PAM are labeled; the deletion mutation sequence is marked in red. (E) T7EN1 cleavage assays performed with genomic DNA from liver samples taken from mice 3 days after receiving Ad.ctrl (lanes 1–5) and Ad.sg126 (lanes 6–10).

(Figure 2E), and there was no evidence of mutagenesis in the Ad.ctrl mice.

Deletion of miR-126a Using the CRISPR/Cas9 System Accelerated the Age-Associated Phenotype in BMSCs

MSCs have been studied for the treatment of liver failure for several years. To establish the role of miR-126a in BMSCs, we next set out to study the function of miR-126a by disruption of its gene in BMSCs, by using the CRISPR/Cas9 system. First, we used a lentiviral vector to derive Ctrl-BMSC and Sg126-BMSC lines. To validate Cas9 and sgRNA expression and function from this lentiviral vector, we used GFP as a reporter. In the presence of Lenti.sg126/Lenti.ctrl infection, almost all cells expressed GFP (Figure S2B). Ctrl-BMSCs and Sg126-BMSCs genomic DNA were isolated after lentivirus infection, and the region around the target site was amplified by PCR. The PCR assay displayed cleavage bands (Figure 3A). The short bands represent a truncated genomic fragment, and the long bands represent the wild-type (WT) case. The T7EN1 cleavage assay showed that samples displayed cleavage bands (Figure 3B). The sequence of PCR products exhibited the deletion of pre-miR-126a and that it was the same as in 3T3-L1 cells (Figure 2D). To further validate the miR-126a gene-editing function of Lenti.sg126. We used a real-time PCR expression analysis of mature miR-126a-3p and -5p in Sg126- and Ctrl-BMSCs. As shown in Figure 3C, miR-126a-3p and -5p expression was significantly downregulated in BMSCs after Lenti.sg126 infection, compared with Lenti.ctrl. These data demonstrated that the designed sgRNA worked well with Cas9 to target pre-miR-126a in BMSCs.

Cellular senescence plays an important role in the complex process of biological aging of tissues, organs, and organisms and is driven by many factors, including oxidative stress, inflammation, DNA damage, and repair responses. We hypothesized that miR-126a would regulate BMSC senescence by regulating telomere length, inflammation, and DNA damage response. As expected, Sg126-BMSCs showed shorter telomeres (Figure 3D) and increased DNA damage responses, as measured by γ-H2A.X levels (Figure 3E). Then, we measured the abundance of NF-κB P65 nuclear protein and found that more P65 translocated to the nucleus in BMSCs after miR-126a deletion (Figure 3F). Signal transducers and activators of transcription 3 (STAT3) is the downstream gene of NF-κB. As shown in Figure 3F, pre-miR-126a disruption dramatically activated P-STAT3 signaling. These data suggest that disruption of miR-126a accelerated age-associated phenotypes and induced proinflammatory cytokines in BMSCs.

VCAN Is a Direct Target of miR-126a-5p

To identify putative mRNA of miR-126a that could contribute to the aging of the liver, we used three miRNA target-prediction tools,

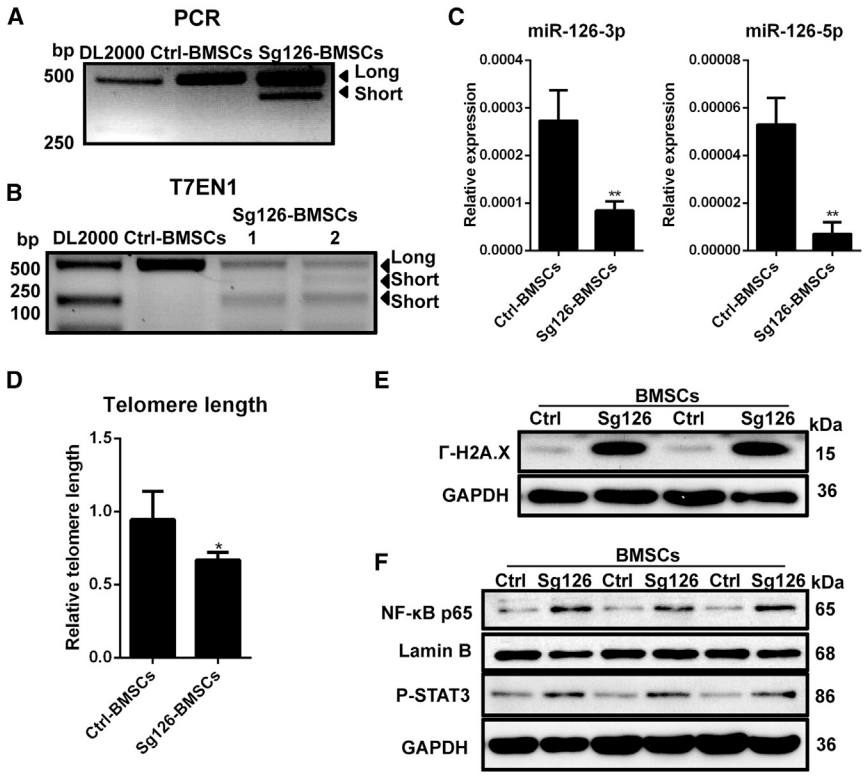

Figure 3. Disruption of miR-126a Using the CRISPR/Cas9 System Accelerated Age-Associated Telomere Shortening, DNA Damage Response, and Inflammation in BMSCs

(A) BMSCs were infected with lentivirus-ctrl (Ctrl-BMSCs) and lentivirus-sg126 (Sg126-BMSCs). Detection of the miR-126a deleted genomic sequence in Ctrl- and Sg126-BMSCs by PCR. (B) Detection of sgRNA: Cas9-mediated on-target cleavage of miR-126, confirmed by T7EN1 cleavage assay in Ctrl- and Sg126-BMSCs. (C) Real-time PCR expression analysis of miR-126a-3p and -5p in Ctrl- and Sg126-BMSCs. U6 snRNA was used as a control for the detection of mature miR-126a-3p and -5p. Bars represent normalized mean values ± SD. $^{**}p < 0.01$ by two-tailed Student's t-test. (D) Real-time PCR-based telomere length measurement of Ctrl- and Sg126-BMSCs. Bars represent normalized mean values ± SD. $^{**}p < 0.01$ by two-tailed Student's t-test. (E and F) Expression of γ-H2A.X (E), and P-STAT3 and nuclear extracts of NF-κB P65 (F) were measured at the protein level in Ctrl- and Sg126-BMSCs. GAPDH was used as the control for the examination of γ-H2A.X and P-STAT3, and Lamin B was used as the control for the examination of NF-κB P65.

including miRanda, PicTar, and Targetscan 7.1. It was found that about 35 targets of miR-126a-3p/miR-126a-5p may be involved in the process of cellular senescence and aging. We then analyzed the expression of approximately 35 targets by qRT-PCR in aged mice (13–16 months old) compared with young mice (8 weeks old). VCAN exhibited more than a 5-fold change in expression levels with a significant p value (Figure 4A).

VCAN plays a role in apoptosis of breast cancer cells and is involved in UV-induced, reactive-oxygen-species-caused accumulation of DNA damage,[24] indicating a potential role in aging. To assess whether VCAN is a direct target of miR-126a-5p, we generated luciferase reporter constructs in which the miR-126a-5p seed target or the VCAN 3′ UTR (WT) was placed behind the luciferase gene (Figure 4B). Meanwhile, the site-mutated sequence (Mut) (Figure 4B) was cloned into the luciferase reporter vector PsiCheck2. Then, the WT or Mut vector was co-transfected with miR-126a-5p mimics or negative control (NC) into HeLa cells. For the VCAN WT vector, significant repression of luciferase activity was induced by co-transfection with miR-126a-5p, in comparison with the control co-transfection.

Moreover, luciferase activity of the VCAN Mut vector or vector only was unaffected by a simultaneous transfection, with either the miR-126a-5p mimics or NC (Figure 4C). In agreement with the post-transcriptional mechanism of action of miRNAs, VCAN was even more profoundly upregulated at the protein level in aged livers (Figure 4A). *In vitro*, compared with Ctrl-BMSCs, Sg126-BMSCs also showed increased VCAN expression, as revealed by qRT-PCR and western blot (Figure 4D). In addition, the WT, Mut vector, or PsiCheck2 was co-transfected with miR-126a-3p mimics or NC into HeLa cells. luciferase activity was unaffected by a simultaneous transfection with either the miR-126a-3p mimics or NC (Figure S3A). VCAN mRNA levels were measured by qRT-PCR after simultaneous transfection of miR-126a-3p mimics, miR-126a-5p mimics, or NC into BMSCs. No significant difference was detected in VCAN mRNA levels after simultaneous transfection of miR-126a-3p mimics or miR-126a-5p mimics (Figures S3B and S3C). VCAN protein levels were measured, and the results showed that VCAN was more profoundly reduced at the protein level after simultaneous transfection of miR-126a-5p mimics (Figure 4E), but not of miR-126a-3p (Figure S3D). Together, these results demonstrate that miR-126a-5p directly targets VCAN, but not miR-126a-3p.

Disruption of miR-126a in Livers Promotes Hepatic Aging and Inhibits Hepatic Function by Targeting VCAN

To further study the role of miR-126a in hepatic aging, we disrupted miR-126a by delivering Ad.sg126 into mouse livers, which reduced liver expression of miR-126a. The changes in miR-126a-3p/miR-126a-5p levels were confirmed by qRT-PCR (Figure S4A). Similar to BMSCs, adenovirus-mediated disruption of miR-126a upregulated VCAN in the liver (Figure 5A). In addition, immunohistochemical (IHC) staining revealed that deletion of miR-126a increased VCAN expression in the liver (Figure 5B). Together, these results demonstrate that miR-126a-5p directly targets VCAN *in vivo*.

As DNA damage responses can be caused by DNA damage as well as telomere dysfunction, we assessed the DNA damage marker γ-H2A.X

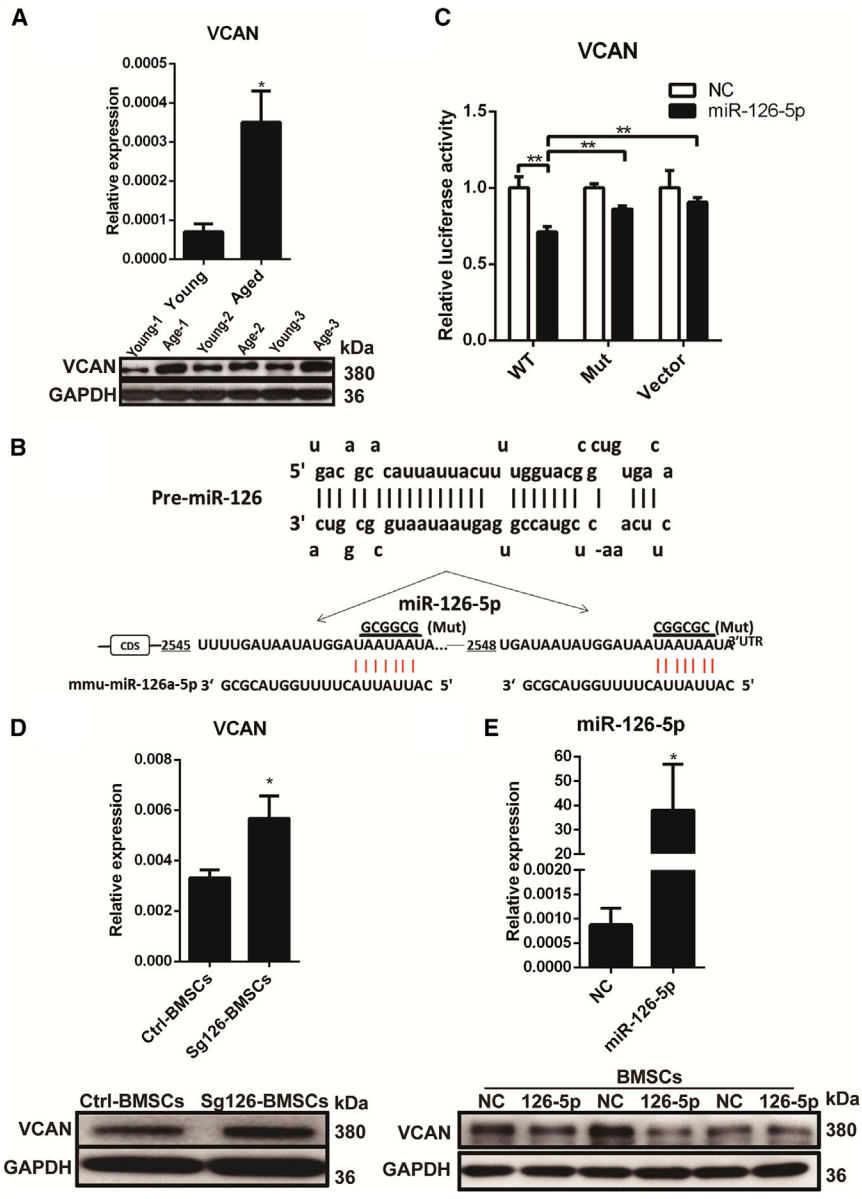

Figure 4. miR-126a-5p Directly Targets VCAN

(A) Real-time PCR expression analysis of VCAN in aged and young mouse livers. Western blot for VCAN protein in aged and young mouse livers. Bars represent normalized mean values ± SD. *p < 0.05 by two-tailed Student's t-test. (B) The 3′ UTR of the VCAN gene contains binding sites for miR-126a-5p according to TargetScan (http://www.targetscan.org/vert_72/). Black underlined sequences show the point mutations used to generate mouse VCAN 3′ UTR Mut constructs. (C) Relative luciferase activity assays of luciferase reporters with WT or mutant VCAN 3′ UTR were performed after co-transfection with miR-126a-5p mimics or NC. The 3′ UTR-Mut indicates the introduction of alterations into the seed complementary sites shown in (B). Bars represent normalized mean values ± SD. **p < 0.01 by two-tailed Student's t-test. (D) Ctrl- and Sg126-BMSCs were collected, and VCAN levels were measured by real-time PCR and western blotting. 36B4 was used as the control for the detection of VCAN by real-time PCR. GAPDH was used as the control for the examination of VCAN by western blot. Bars represent normalized mean values ± SD. *p < 0.05 by two-tailed Student's t-test. (E) miR-126a-5p mRNA levels were measured by real-time PCR after simultaneous transfection of miR-126a-5p mimics or NC. VCAN protein levels were measured by western blotting after simultaneous transfection of miR-126a-5p mimics or NC. U6 was used as a control for the detection of miR-126a-5p by real-time PCR. GAPDH was used as a control for the examination of VCAN by western blot. Bars represent normalized mean values ± SD. *p < 0.05 by two-tailed Student's t-test.

and telomere length in livers. Disruption of miR-126a induced DNA damage in livers, as measured by telomere length (Figure 5C) and γ-H2A.X levels (Figure 5D). To test whether miR-126a contributes to hepatic dysfunction after disruption of miR-126a in the liver, we euthanized the mice to harvest blood. We found that plasma levels of aspartate aminotransferase (AST) and alanine aminotransferase (ALT) were significantly upregulated after disruption of miR-126a (Figure 5E).

After adenovirus-mediated sg126 injection, hepatic steatosis was slightly induced on day 3 in Ad.sg126 mouse liver, compared with control mouse liver. This was apparently related to an augmented increase in triglyceride (TRIG) and cholesterol (CHOL) accumulation in the livers of miR-126a-knockdown mice (Figure 5F). The hepatocyte-like cells contained medium vacuoles in Ad.sg126 mouse livers compared with Ad.ctrl mouse livers. These vacuoles were positive via Oil Red O staining (Figure S4B). Histological examination of the liver was performed, and the data demonstrated that liver structure integrity and cell arrangements were uniform in the control adenovirus and PBS groups, but the Ad.sg126 group had extensive liver damage, liver tissue edema, cell arrangement disorders, and pyramidal nucleus pyknosis (Figure 5G). These findings indicate that miR-126a has favorable effects on the aging process in the liver and hepatic function by targeting VCAN in the hepatic miR-126a gene-deletion model.

Disruption of miR-126a in BMSCs Accelerated Age-Related Phenotypes and Decreased Their Therapeutic Effects against Cirrhosis by Targeting VCAN

To further examine the role of VCAN in the BMSC aging process, we determined whether VCAN promotes telomere attrition of BMSCs. In the VCAN-silenced BMSCs, the disruption of miR-126a-mediated telomere attrition was abrogated (Figure 6A). To assess whether

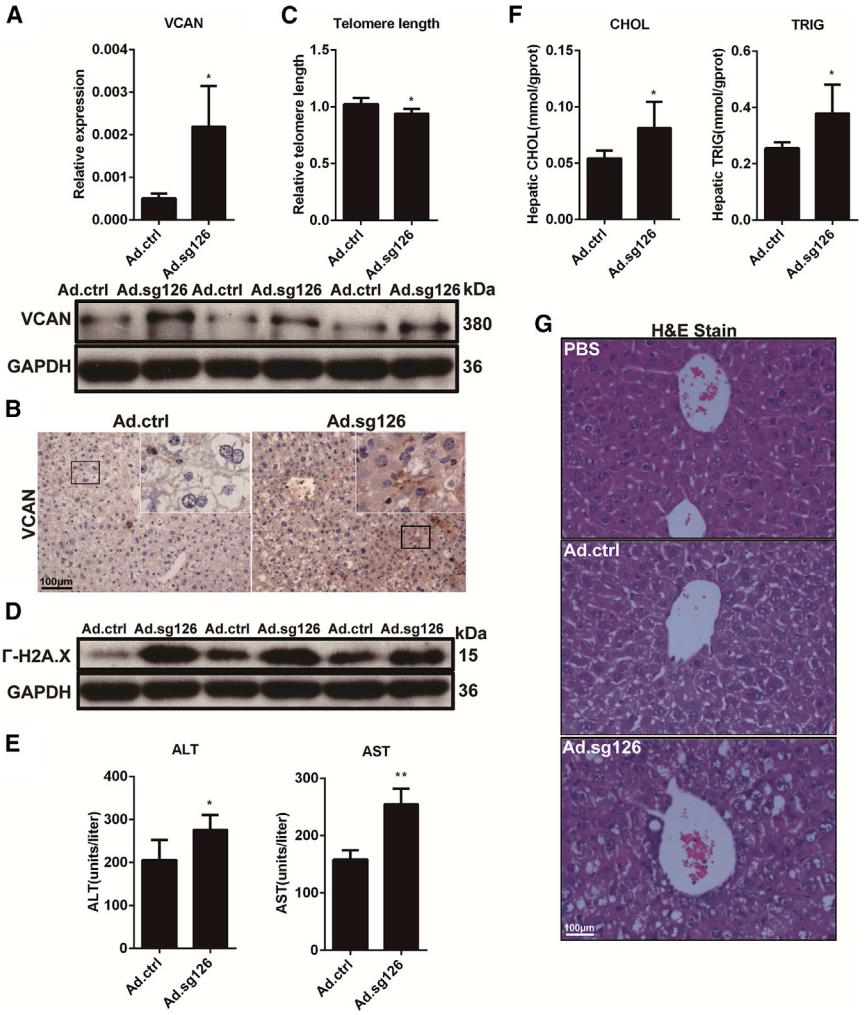

Figure 5. Deletion of miR-126a in Livers Promotes Hepatic Aging and Inhibits Hepatic Metabolism by Targeting VCAN

(A) VCAN levels were measured by real-time PCR and western blotting in livers of Ad.ctrl and Ad.sg126 mice. Bars represent normalized mean values ± SD. *$p < 0.05$ by two-tailed Student's t-test. (B) VCAN levels were measured by IHC staining in livers of Ad.ctrl and Ad.sg126 mice. (C) Real-time PCR-based telomere length measurement in livers of Ad.ctrl and Ad.sg126 mice. Bars represent normalized mean values ± SD. *$p < 0.05$ by two-tailed Student's t-test. (D) Expression of γ-H2A.X was measured at the protein level in Ad.ctrl and Ad.sg126 mouse livers. GAPDH was used as a control for γ-H2A.X. (E) Plasma ALT and AST levels of the Ad.ctrl and Ad.sg126 mice 3 days after receiving the adenovirus. Bars represent normalized mean values ± SD. *$p < 0.05$, **$p < 0.01$ by two-tailed Student's t-test. (F) Triglyceride (TRIG) and cholesterol (CHOL) levels in the livers of Ad.ctrl and Ad.sg126 mice 3 days after they received the adenovirus. Bars represent normalized mean values ± SD. *$p < 0.05$ by two-tailed Student's t-test. (G) Representative H&E staining in PBS mouse livers and in Ad.ctrl and Ad.sg126 mouse livers 3 days after intravenous tail injection.

VCAN is involved in senescence-associated inflammation in BMSCs, we transfected Sg126-BMSCs or Ctrl-BMSCs with VCAN siRNA. As shown in Figures 6B and 6C, the effect of VCAN silencing rescued the disruption of miR-126a-mediated promotion of inflammation, as revealed by qRT-PCR and western blot, suggesting that VCAN is one of the most important target genes of miR-126a-5p.

Our finding that miR-126a regulates telomere length and DNA damage responses prompted us to further investigate the pro-senescence effect of the target gene VCAN in BMSCs. We observed that disruption of miR-126a in BMSCs caused senescence-like phenotypes, with positive staining for SA-β-gal, and that silencing of VCAN resulted in decreased expression of SA-β-gal (Figure 6D). Together, these data show that miR-126a inhibits telomere attrition and cell senescence and weakens senescence-induced inflammation in BMSCs by targeting VCAN.

We next studied the role of miR-126a in BMSCs *in vivo* using the bile duct ligation (BDL) liver fibrosis model. Mice were subjected to a BDL procedure to induce liver cirrhosis. After 3 weeks, the mice underwent BMSC cell transplantation by injection of 100 μL of a Sg126-BMSC or Ctrl-BMSC suspension (1.0×10^4 cells/μL suspended in PBS). Liver tissue and blood were harvested and analyzed 1 week after transplantation. As shown in Figure 6E, the α-smooth muscle actin (α-SMA, a myofibroblast marker) levels in the liver were significantly increased in the mice that received Sg126-BMSCs, compared with those that received Ctrl-BMSCs. These results implied that injecting Sg126-BMSCs into cirrhotic liver contributed to hepatic dysfunction. These findings were confirmed by analysis of fibrosis in histological sections of the livers stained with H&E and Masson's trichrome (Figure 6F). The results showed that liver damage was repaired after transplantation of Ctrl-BMSCs, compared with the BDL control group. However, liver damage in the mice was aggravated after transplantation of Sg126-BMSCs, compared with those that received Ctrl-BMSCs. The percentage area of Masson's trichrome staining in each group was calculated. As shown in Figure 6F, the Sg126-BMSCs group exhibited an approximately 2.5-fold increase of fibrotic tissue area compared with that of the Ctrl-BMSC group. Taken together, these results suggest that decreased expression of miR-126a in BMSCs will affect its rescue function in the treatment of chronic liver failure.

In summary, this study demonstrated that miR-126a participates in hepatic aging and function by targeting VCAN, and deletion of miR-126a using the CRISPR/Cas9 system accelerated aging, induced pro-inflammatory cytokines in BMSCs, and decreased their

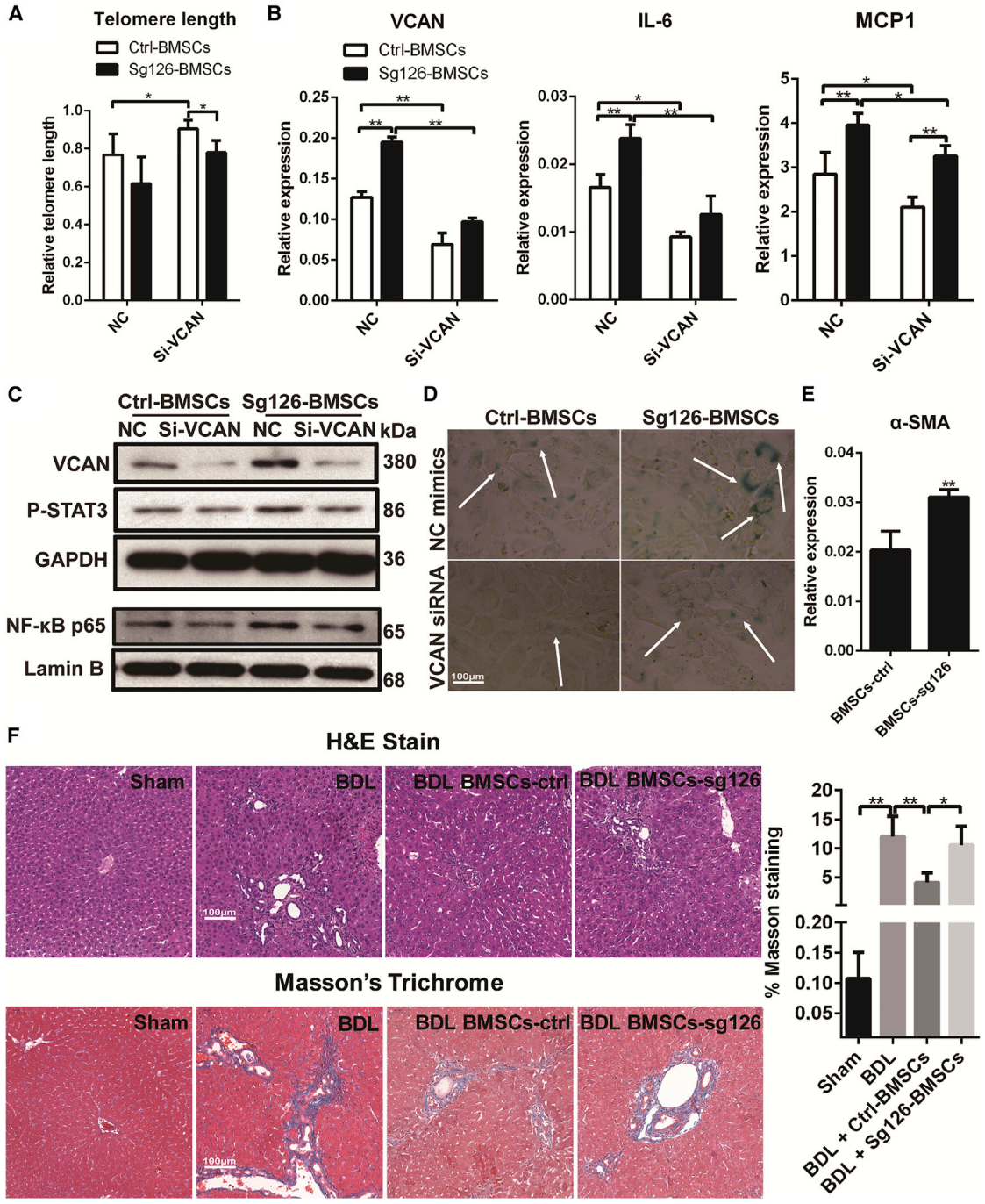

Figure 6. Disruption of miR-126a in BMSCs Accelerated the Age-Related Phenotype and Inflammation and Decreased Their Therapeutic Effects against Cirrhosis by Targeting VCAN

(A) Quantification by qRT-PCR of miR-126a and VCAN effects on telomere length. Bars represent normalized mean values ± SD. *$p < 0.05$ by two-tailed Student's t-test. (B) Ctrl- and Sg126-BMSCs were transfected with the VCAN siRNA or NC for 48 h, and the expression levels of VCAN, MCP-1, and IL-6 were assayed using real-time PCR. 36B4 was used as the control. Bars represent normalized mean values ± SD. *$p < 0.05$, **$p < 0.01$ by two-tailed Student's t-test. (C) Ctrl- and Sg126-BMSCs were transfected with VCAN siRNA or NC. VCAN, P-STAT3, and nuclear extract NF-κB P65 levels were measured by western blotting. GAPDH was used as a control for VCAN and P-STAT3, and Lamin B was used as a control for NF-κB P65. (D) The effects of miR-126a-5p knockdown and VCAN silencing on cellular senescence were analyzed by SA-β-gal expression. (E) Real-time PCR expression analysis of α-SMA in defective mouse livers at 7 days after transplantation of

(legend continued on next page)

therapeutic effects against cirrhosis. Further *in vivo* research indicated that deletion of miR-126a in livers promoted hepatic aging and damage and inhibited hepatic function by targeting VCAN.

DISCUSSION

Previous research has shown that targeted deletion of miR-126 in mice results in embryonic lethality in a subset of mutant mice[17] and that miR-126 is a regulator of skin aging.[25] In this study, miR-126a was dramatically decreased in aged mice, and disruption of miR-126a gene promoted hepatic aging and inflammation.

Our results showed that miR-126a abundance was significantly lower in aged livers than in young livers, and this age-related reduction of miR-126a was accompanied by shorter telomeres and decreased TERT expression in livers. In line with our experimental findings, telomere reduction occurs in human liver tissues with age and chronic inflammation.[26,27] This suggests that miR-126a contributes to hepatic aging and hepatic function. Thus, whether miR-126a could be used in the early detection of hepatic aging or damage may be a future direction of study to increase the sensitivity of assessing hepatic function and disease.

Chronic inflammation is believed to be one of the major causes of liver cancer development, and inhibition of inflammation is one target for preventing aging-related diseases.[28–30] miR-126a has been shown to suppress inflammation in endothelial cells under hyperglycemic conditions.[31] Consistent with the previous report, our results showed that miR-126a antagonizes the NF-κB signaling pathway and thus contributes to the repair of damaged liver tissues and promotes liver health.

To demonstrate the biological functions and molecular mechanisms of miR-126a in the liver, CRISPR/Cas9-mediated genome editing *in vivo* using viral delivery was applied in our study. CRISPR/Cas9 mediates knockdown by deleting the coding sequence rather than by acting at the level of RNA.[32] Although they enable rapid CRISPR-based editing to produce gene modifications and chromosomal rearrangements, such methodologies are restricted to those tissues that can be efficiently accessed by exogenous constructs.[33] Specifically, adenovirus vectors have been shown to have a predilection for liver and lung.[34] Therefore, in this study, we used an adenovirus vector to deliver a CRISPR/Cas9 system targeting miR-126a in mouse livers and a lentivirus vector to deliver a CRISPR/Cas9 system targeting miR-126a in BMSCs. All of the systems had high deletion efficiency in BMSCs and in the liver.

BMSCs have been widely used in the treatment of fibrotic diseases. Previous research has shown that miR-126a has an important role in mesenchymal stem cells (MSCs) in breast cancer metastasis, independently suppressing the sequential recruitment of MSCs and inflammatory monocytes into the tumor stroma to inhibit lung metastasis by breast tumor cells,[16] and these results are consistent with our findings that miR-126a has abundant expression in BMSCs (Figure S2A). However, further enhancement of their power in tissue repair and regeneration could facilitate their application. Thus, some recent reports have approached gene expression of MSCs through miRNA intervention.[35] In this study, we used lentivirus vectors to deliver a CRISPR/Cas9 system targeting miR-126a, which we transduced into BMSCs, and found that disruption of miR-126a accelerated senescence and inflammation in the cells and promoted a DNA damage response. After transplanting these transduced cells into liver-defective mice, we found that the contribution of BMSCs to liver repair was attenuated. Therefore, miR-126a was associated with the function of transplanted BMSCs in liver repair.

Liver repair and regeneration are of prime importance for the maintenance of liver homeostasis during aging.[36] Here, we show that disruption of miR-126a using the CRISPR/Cas9 adenovirus system in mouse liver promoted telomere shortening, a DNA damage response, and NF-κB activity. To further substantiate the role of miR-126a in hepatic aging phenotypes, we analyzed hepatic steatosis and fibrosis in histological sections of livers. Our results showed that livers with adenovirus-mediated miR-126a deletion had more hepatocyte necrosis and steatosis and showed more inflammatory cells, compared with control livers. These findings indicate that high levels of miR-126a are critical for liver repair.

The contribution of BMSCs to liver repair varies considerably, and recent evidence has suggested that these cells contribute to liver fibrosis repair.[37] In this study, we showed an important phenotypic similarity between knockdown of miR-126a-5p expression and silencing of VCAN in BMSCs. Importantly, the effects of knockdown of miR-126a-5p in BMSCs were telomere shortening, senescence-like phenotypes, and inflammation, which were rescued by the silencing of VCAN, indicating that VCAN is a central mediator for the effects of miR-126a-5p in BMSCs. Our results showed that disruption of miR-126a-5p caused activation of the NF-κB pathway, and silencing of VCAN reversed the effect. These results suggest that miR-126a-5p can release VCAN's promotion role and inhibit the NF-κB pathway, contributing to hepatic aging and inflammation.

In summary, our data demonstrate that disruption of miR-126a increases age-induced hepatic damage and functional decline *in vivo*. Moreover, disruption of miR-126a weakens hepatic metabolism. miR-126a-5p suppresses the expression of VCAN, which induces telomere erosion, cell senescence, and inflammation, thus providing a rationale for the anti-aging effects of miR-126a in the hepatic cell or BMSCs. In addition to VCAN, miR-126a-5p has other targets,

Ctrl-BMSCs (BMSCs-ctrl group) and Sg126-BMSCs (BMSCs-sg126 group). 36B4 was used as a control for α-SMA. Bars represent normalized mean values ± SD. **$p < 0.01$ by two-tailed Student's t-test. (F) Representative H&E and Masson's trichrome staining of BMSCs-Ctrl and BMSCs-sg126 mouse livers 7 days after transplantation of BMSCs. The percentage area of Masson's trichrome staining in each group was calculated. Bars represent normalized mean values ± SD. *$p < 0.05$, **$p < 0.01$ by two-tailed Student's t-test.

such as delta-like 1 homolog (Dlk1), that impairs angiogenesis by inhibiting endothelial cell proliferation and promotes atherosclerosis.[38] Nevertheless, we demonstrated that the miR-126a-5p-VCAN axis has profound effects on hepatic aging and function and the therapeutic effects of BMSCs against cirrhosis, indicating that VCAN is a key downstream effector of miR-126a-5p. Moreover, our findings that VCAN is induced in aging and regulates telomere attrition and senescence-associated inflammation provide a plausible mechanism by which pro-inflammatory responses occur during aging.

Finally, our results show that administration of miR-126a-5p is a potential therapeutic strategy to improve hepatic repair and metabolism function after hepatic damage and disease. Meanwhile, the administration of miR-126a-5p also improves the rescue effect of BMSC transplantation in hepatic damage and disease. This principal finding may have a clinical impact in treating liver diseases.

MATERIALS AND METHODS

Cell Culture, Infection, and miRNA Transfection

The cell lines used in this study were *HEK293A*, *HEK293T*, *BMSC*, *HeLa*, *NIH 3T3*, and *3T3-L1*. All cell lines were cultured in DMEM (Hyclone, Logan, UT, USA) with 10% fetal bovine serum (FBS; Gibco BRL, Grand Island, NY, USA) and penicillin-streptomycin. Cells were seeded in 24-well plates 24 h before being infected with Ad.ctrl and Ad.sg126 or Lenti.ctrl and Lenti.sg126. miRNAs were transfected at a concentration of 30 nM using Lipofectamine RNAiMAX (Invitrogen, Carlsbad, CA, USA) according to the manufacturer's instructions. The miR-126a-5p mimics, NCs, and VCAN siRNA were all purchased from Gene Pharma (Shanghai, China). The primer sequences are listed in Table S1.

Animals

Adult *C57BL/6J* male mice (8 weeks old) and aged mice (13–16 months old) were housed in a pathogen-free animal facility under a standard 12-hour light/dark cycle. Mice were given standard rodent chow and water *ad libitum*. Adult *C57BL/6J* male mice were divided randomly into four groups, and bile duct ligation in the mice was performed as previously described.[39] BMSCs obtained from *C57BL/6J* male mice (6 weeks old) were isolated and cultured according to an established protocol.[40] On post-operative day 23, 1×10^6 of Lenti.ctrl and Lenti.sg126 preconditioned BMSCs were injected via the caudal vein. Ad.sg126 mice and Ad.ctrl mice (*C57BL/6J* background) were generated using recombination Ad.sg126 or Ad.ctrl (Hanbio, Shanghai, China). Viral particles (1.0×10^{10}) were reconstituted in 100 μL injected intravenously through the tail vein with BD Ultra-Fine Insulin Syringes. All procedures followed the Huazhong Agricultural University Guidelines for the Care and Use of Laboratory Animals.

Identification of Potential Downstream Targets of miR-126a

The potential downstream targets of miR-126a were identified using three *in silico* analysis programs: MicroRNA.org (http://www.mirbase.org/cgi-bin/mirna_entry.pl?acc=MI0000153), TargetScan (http://www.targetscan.org/vert_72/), and PicTar (https://pictar.mdc-berlin.de/).

miRNA, mRNA Extraction, and qPCR

The RNAiso Plus (Takara, Japan) was used to isolate total RNA, including low-molecular-weight RNA from frozen samples and cell lines, according to the manufacturer's protocol. We used SYBR-based RT-PCR (ToYoBo, Japan) to quantify mature miRNA expression for miR-126a-5p, miR-126a-3p, or U6 (Applied Biosystems, USA). The relative levels were calculated using the comparative-Ct method ($2^{-\Delta\Delta Ct}$ method). The primer sequences are listed in Table S2.

Luciferase Reporter Assay

Luciferase constructs were made by inserting the mouse VCAN 3′ UTR, obtained from imagenes, into the psiCheck2 vector (Promega), in which the putative miR-126a-5p seed sequence-binding site, 5′-TAATAATA-3′, was mutated to 5′-CGGCGCTA-3′. The primer sequences are listed in Table S3. Forty-eight hours after transfection, firefly and *Renilla* luciferase activities were measured with the Dual Luciferase Reporter Assay System (Promega). The *Renilla* luciferase activity was normalized to the Firefly luciferase activity.

Analysis of ALT, AST, TRIG, and CHOL

Plasma was collected from blood after centrifugation at 3,000 rpm for 10 min at 4°C. Plasma ALT and AST were detected by using commercial kits (Nanjing Jiancheng Bio-engineering Institute) according to the manufacturer's instructions. For hepatic TRIG and CHOL measurement, frozen livers were homogenized in PBS. Supernatant was collected from lysates after centrifugation at 2,500 rpm for 10 min at 4°C. The hepatic TRIG and CHOL levels in the supernatant were assayed with a kit from the Nanjing Jiancheng Bio-engineering Institute.

Senescence-Associated β-Galactosidase Staining

BMSC senescence was determined by *in situ* staining for senescence-associated β-galactosidase (SA-β-gal), with a senescence cell histochemical staining kit (Beyotime), according to the manufacturer's instructions. Images of the staining were taken from 5–10 random microscopic fields per sample at ×200 magnification.

PCR and T7EN1 Cleavage Assay and Sequencing

Genomic DNA was isolated from liver tissues or cells as described above. PCR, the T7EN1 cleavage assay, and sequencing were performed as described previously. Primer sequences for amplifying the targeted fragments are listed in Table S1. The PCR products were denatured and re-annealed in NE Buffer 2 (New England Biolabs, Ipswich, MA, USA) in a thermocycler. The PCR products were digested with T7EN1 (M0302L; New England Biolabs) for 30 min at 37°C and separated by 1.5% agarose gel electrophoresis. The PCR products with mutations detected by the sequencing were sub-cloned into the pMD 18-T Vector (6011; Takara Bio, Japan). Colonies for each sample were picked up randomly and sequenced with the M13 Primer (5′-CGCCAGGGTTTTCCCAGTCACGAC-3′).

Plasmid Construction and Lentivirus and Adenovirus Production

To completely delete miR-126a *in vitro* and *in vivo*, we designed three sgRNAs around the locus of miR-126a and used them in pairs, as it has been shown that paired sgRNAs can generate large-fragment deletion. Sg1 and sg3 are on the 3′ terminus of miR-126a, whereas sg2 is on its 5′ terminus. After targeting efficiency was confirmed in the NIH 3T3 cell line, the cells were cloned into lentivirus and adenovirus plasmids. The lentivirus plasmids were constructed based on lentiCRISPRv2 (cat. no. 98290; Addgene), in which we replaced the hSpCas9 with our own spCas9-GFP fusion sequence. The sgRNAs derived by dual U6 promoters were inserted in front of the EFS-NS promoter. They were named Lenti.sg126(1+2) or Lenti.sg126(3+2) and Lenti.ctrl. The resulting lentivirus vector was packaged and transduced into HEK293T cells. For recombinant adenovirus construction, the sgRNAs and spCas9-GFP fragments were cloned into entry vectors. Gateway Cloning Technology was used for the final recombination into destination vectors, which were named Ad.sg126(3+2) and Ad.ctrl. They were transfected into HEK293 cells by using Lipofectamine 2000 transfection reagent (Invitrogen, Carlsbad, CA), to generate the recombinant adenoviruses. Ad.sg126 and Ad.ctrl (Hanbio, Shanghai, China) were propagated in HEK293 cells. The propagated recombinant adenoviruses in the HEK293 cells were purified, and the titer of virus was measured by plaque assays. The stock solutions of Ad.sg126 and Ad.ctrl were 1×10^{10} plaque formation units (PFU)/mL.

Liver Histology and Immunohistochemical Staining

Livers were fixed in 4% PBS-buffered formalin, dehydrated, embedded in paraffin, sectioned at 5 μm, and processed for H&E and Masson's trichrome IHC staining. For the IHC assay, slides were incubated with biotin-label goat anti-rabbit IgG, followed by horseradish peroxidase (HRP), to label streptavidin.

DNA Extraction and Measurement of Telomere Length

Genomic DNA was isolated from liver tissues or BMSCs with DNA isolation buffer (10 mM Tris-HCl, 100 mM NaCl, 10 mM EDTA, and 0.5% SDS) and recovered by alcohol precipitation. Relative mean telomere length was determined by RT-PCR measurement of the ratio of telomere repeat units (Tel) to a single-copy gene (CON, 36B4), as described previously.[41] The primer sequences are listed in Table S4.

Western Blot

For whole-cell protein extraction, liver tissues were prepared in lysis buffer (Beyotime, China) according to the manufacturer's instructions. For nuclear protein extraction, cells were lysed in cytoplasm extraction buffer A and B (BestBio, Shanghai, China), according to the manufacturer's instructions. The antibody (Ab) against TERT was purchased from Santa Cruz Biotechnology (Santa Cruz, CA). The Ab against GAPDH was purchased from Boster (Wuhan, China). The Abs against γ-H2A.X, NF-κB p65, and P-STAT3 were purchased from Cell Signaling Technology (Danvers, MA, USA). The Ab against Lamin B was purchased from Proteintech (Chicago, IL, USA). The Ab against VCAN was purchased from Abcam (Cambridge, UK).

Statistical Analysis

All data represent at least three independent experiments and are expressed as the mean ± SD. A two-tailed Student's t-test was used to calculate p values. $p < 0.05$ was considered significant.

For *in vitro* and *in vivo* experiments, the data were collected randomly, and the samples were appropriately blocked.

SUPPLEMENTAL INFORMATION

Supplemental Information can be found online at https://doi.org/10.1016/j.omtn.2019.04.002.

AUTHOR CONTRIBUTIONS

Y.Y., L.Z., X.H., W.H., D.W., L.W., and X.C.: study concept and design; Y.Y.: acquisition of experimental data; Y.Y., S.L., and D.Q.: biliary ligation surgery procedures; C.Z.: assistance in molecular assays; B.H.: construction of adenovirus and lentiviral vectors; Y.Y. and D.Q.: BMSC transplantation; D.Q., B.H., L.W., and X.C.: discussions and manuscript review; Y.Y.: draft manuscript writing; and L.Z.: data organization and writing.

CONFLICTS OF INTEREST

The authors declare no competing interests.

ACKNOWLEDGMENTS

This work was supported by National Key R&D Plan no. 2017YFA0103202 and no. 2017YFA0103200, the Fundamental Research Funds for the Central Universities (2662017PY106, 2662016PY087, and 2662019YJ008), the Youth 1000 Plan Project and Huazhong Agricultural University Startup funds to L.Z.

REFERENCES

1. Bartel, D.P. (2004). MicroRNAs: genomics, biogenesis, mechanism, and function. Cell *116*, 281–297.
2. Esteller, M. (2011). Non-coding RNAs in human disease. Nat. Rev. Genet. *12*, 861–874.
3. Yates, L.A., Norbury, C.J., and Gilbert, R.J. (2013). The long and short of microRNA. Cell *153*, 516–519.
4. Zhang, L., Yang, L., Liu, X., Chen, W., Chang, L., Chen, L., Loera, S., Chu, P., Huang, W.C., Liu, Y.R., and Yen, Y. (2013). MicroRNA-657 promotes tumorigenesis in hepatocellular carcinoma by targeting transducin-like enhancer protein 1 through nuclear factor kappa B pathways. Hepatology *57*, 1919–1930.
5. Baek, D., Villén, J., Shin, C., Camargo, F.D., Gygi, S.P., and Bartel, D.P. (2008). The impact of microRNAs on protein output. Nature *455*, 64–71.
6. Cheng, Y., Wei, Z., Xie, S., Peng, Y., Yan, Y., Qin, D., Liu, S., Xu, Y., Li, G., and Zhang, L. (2017). Alleviation of Toxicity Caused by Overactivation of Pparα through Pparα-Inducible miR-181a2. Mol. Ther. Nucleic Acids *9*, 195–206.
7. Boehm, M., and Slack, F. (2005). A developmental timing microRNA and its target regulate life span in C. elegans. Science *310*, 1954–1957.
8. Zhang, Y., Kim, M.S., Jia, B., Yan, J., Zuniga-Hertz, J.P., Han, C., and Cai, D. (2017). Hypothalamic stem cells control ageing speed partly through exosomal miRNAs. Nature *548*, 52–57.
9. Epstein, Y., Perry, N., Volin, M., Zohar-Fux, M., Braun, R., Porat-Kuperstein, L., and Toledano, H. (2017). miR-9a modulates maintenance and ageing of Drosophila germline stem cells by limiting N-cadherin expression. Nat. Commun. *8*, 600.
10. Boon, R.A., Iekushi, K., Lechner, S., Seeger, T., Fischer, A., Heydt, S., Kaluza, D., Tréguer, K., Carmona, G., Bonauer, A., et al. (2013). MicroRNA-34a regulates cardiac ageing and function. Nature *495*, 107–110.

11. He, C., Shi, Y., Wu, R., Sun, M., Fang, L., Wu, W., Liu, C., Tang, M., Li, Z., Wang, P., et al. (2016). miR-301a promotes intestinal mucosal inflammation through induction of IL-17A and TNF-α in IBD. Gut *65*, 1938–1950.
12. Yu, B., Chang, J., Liu, Y., Li, J., Kevork, K., Al-Hezaimi, K., Graves, D.T., Park, N.H., and Wang, C.Y. (2014). Wnt4 signaling prevents skeletal aging and inflammation by inhibiting nuclear factor-κB. Nat. Med. *20*, 1009–1017.
13. Smith-Vikos, T., and Slack, F.J. (2012). MicroRNAs and their roles in aging. J. Cell Sci. *125*, 7–17.
14. Serrano, M., Lin, A.W., McCurrach, M.E., Beach, D., and Lowe, S.W. (1997). Oncogenic ras provokes premature cell senescence associated with accumulation of p53 and p16INK4a. Cell *88*, 593–602.
15. Collado, M., Blasco, M.A., and Serrano, M. (2007). Cellular senescence in cancer and aging. Cell *130*, 223–233.
16. Zhang, Y., Yang, P., Sun, T., Li, D., Xu, X., Rui, Y., Li, C., Chong, M., Ibrahim, T., Mercatali, L., et al. (2013). miR-126 and miR-126* repress recruitment of mesenchymal stem cells and inflammatory monocytes to inhibit breast cancer metastasis. Nat. Cell Biol. *15*, 284–294.
17. Wang, S., Aurora, A.B., Johnson, B.A., Qi, X., McAnally, J., Hill, J.A., Richardson, J.A., Bassel-Duby, R., and Olson, E.N. (2008). The endothelial-specific microRNA miR-126 governs vascular integrity and angiogenesis. Dev. Cell *15*, 261–271.
18. Valdmanis, P.N., Gu, S., Chu, K., Jin, L., Zhang, F., Munding, E.M., Zhang, Y., Huang, Y., Kutay, H., Ghoshal, K., et al. (2016). RNA interference-induced hepatotoxicity results from loss of the first synthesized isoform of microRNA-122 in mice. Nat. Med. *22*, 557–562.
19. Thomas, A.M., Hart, S.N., Kong, B., Fang, J., Zhong, X.B., and Guo, G.L. (2010). Genome-wide tissue-specific farnesoid X receptor binding in mouse liver and intestine. Hepatology *51*, 1410–1419.
20. Chen, W.D., Wang, Y.D., Zhang, L., Shiah, S., Wang, M., Yang, F., Yu, D., Forman, B.M., and Huang, W. (2010). Farnesoid X receptor alleviates age-related proliferation defects in regenerating mouse livers by activating forkhead box m1b transcription. Hepatology *51*, 953–962.
21. Wight, T.N., and Merrilees, M.J. (2004). Proteoglycans in atherosclerosis and restenosis: key roles for versican. Circ. Res. *94*, 1158–1167.
22. Evanko, S.P., Potter-Perigo, S., Bollyky, P.L., Nepom, G.T., and Wight, T.N. (2012). Hyaluronan and versican in the control of human T-lymphocyte adhesion and migration. Matrix Biol. *31*, 90–100.
23. Xia, L., Huang, W., Tian, D., Zhang, L., Qi, X., Chen, Z., Shang, X., Nie, Y., and Wu, K. (2014). Forkhead box Q1 promotes hepatocellular carcinoma metastasis by transactivating ZEB2 and VersicanV1 expression. Hepatology *59*, 958–973.
24. Kunisada, M., Yogianti, F., Sakumi, K., Ono, R., Nakabeppu, Y., and Nishigori, C. (2011). Increased expression of versican in the inflammatory response to UVB- and reactive oxygen species-induced skin tumorigenesis. Am. J. Pathol. *179*, 3056–3065.
25. Fiedler, J., Gronniger, E., Pfanne, A., Bronneke, S., Schmidt, K., Falk, C.S., et al. (2016). Identification of miR-126 as a new regulator of skin aging. Exp. Dermatol. *26*, 284–286.
26. Armanios, M. (2013). Telomeres and age-related disease: how telomere biology informs clinical paradigms. J. Clin. Invest. *123*, 996–1002.
27. Verma, S., Tachtatzis, P., Penrhyn-Lowe, S., Scarpini, C., Jurk, D., Von Zglinicki, T., Coleman, N., and Alexander, G.J. (2012). Sustained telomere length in hepatocytes and cholangiocytes with increasing age in normal liver. Hepatology *56*, 1510–1520.
28. Pikarsky, E., Porat, R.M., Stein, I., Abramovitch, R., Amit, S., Kasem, S., Gutkovich-Pyest, E., Urieli-Shoval, S., Galun, E., and Ben-Neriah, Y. (2004). NF-kappaB functions as a tumour promoter in inflammation-associated cancer. Nature *431*, 461–466.
29. Hoare, M., Das, T., and Alexander, G. (2010). Ageing, telomeres, senescence, and liver injury. J. Hepatol. *53*, 950–961.
30. Aravinthan, A.D., and Alexander, G.J.M. (2016). Senescence in chronic liver disease: Is the future in aging? J. Hepatol. *65*, 825–834.
31. Tang, S.T., Wang, F., Shao, M., Wang, Y., and Zhu, H.Q. (2017). MicroRNA-126 suppresses inflammation in endothelial cells under hyperglycemic condition by targeting HMGB1. Vascul. Pharmacol. *88*, 48–55.
32. Chen, Y., Cui, Y., Shen, B., Niu, Y., Zhao, X., Wang, L., Wang, J., Li, W., Zhou, Q., Ji, W., et al. (2015). Germline acquisition of Cas9/RNA-mediated gene modifications in monkeys. Cell Res. *25*, 262–265.
33. Shen, B., Zhang, J., Wu, H., Wang, J., Ma, K., Li, Z., Zhang, X., Zhang, P., and Huang, X. (2013). Generation of gene-modified mice via Cas9/RNA-mediated gene targeting. Cell Res. *23*, 720–723.
34. Rainov, N.G., Ikeda, K., Qureshi, N.H., Grover, S., Herrlinger, U., Pechan, P., Chiocca, E.A., Breakefield, X.O., and Barnett, F.H. (1999). Intraarterial delivery of adenovirus vectors and liposome-DNA complexes to experimental brain neoplasms. Hum. Gene Ther. *10*, 311–318.
35. Li, C.X., and Talele, N.P. (2017). MicroRNA-21 preserves the fibrotic mechanical memory of mesenchymal stem cells. Nat. Mater. *16*, 379–389.
36. Jurk, D., Wilson, C., Passos, J.F., Oakley, F., Correia-Melo, C., Greaves, L., Saretzki, G., Fox, C., Lawless, C., Anderson, R., et al. (2014). Chronic inflammation induces telomere dysfunction and accelerates ageing in mice. Nat. Commun. *2*, 4172.
37. Li, C., Kong, Y., Wang, H., Wang, S., Yu, H., Liu, X., Yang, L., Jiang, X., Li, L., and Li, L. (2009). Homing of bone marrow mesenchymal stem cells mediated by sphingosine 1-phosphate contributes to liver fibrosis. J. Hepatol. *50*, 1174–1183.
38. Schober, A., Nazari-Jahantigh, M., Wei, Y., Bidzhekov, K., Gremse, F., Grommes, J., Megens, R.T., Heyll, K., Noels, H., Hristov, M., et al. (2014). MicroRNA-126-5p promotes endothelial proliferation and limits atherosclerosis by suppressing Dlk1. Nat. Med. *20*, 368–376.
39. Ding, B.S., Cao, Z., Lis, R., Nolan, D.J., Guo, P., Simons, M., Penfold, M.E., Shido, K., Rabbany, S.Y., and Rafii, S. (2014). Divergent angiocrine signals from vascular niche balance liver regeneration and fibrosis. Nature *505*, 97–102.
40. Makino, S., Fukuda, K., Miyoshi, S., Konishi, F., Kodama, H., Pan, J., Sano, M., Takahashi, T., Hori, S., Abe, H., et al. (1999). Cardiomyocytes can be generated from marrow stromal cells in vitro. J. Clin. Invest. *103*, 697–705.
41. Cawthon, R.M. (2002). Telomere measurement by quantitative PCR. Nucleic Acids Res. *30*, e47.